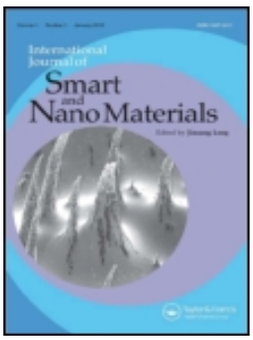

International Journal of Smart and Nano Materials

ISSN: 1947-5411 (Print) 1947-542X (Online) Journal homepage: http://www.tandfonline.com/loi/tsnm20

Electrochemical properties of MnO_2/CNT nanocomposite in neutral aqueous electrolyte as cathode material for asymmetric supercapacitors

Hui Xia & Chao Huo

To cite this article: Hui Xia & Chao Huo (2011) Electrochemical properties of MnO_2/CNT nanocomposite in neutral aqueous electrolyte as cathode material for asymmetric supercapacitors, International Journal of Smart and Nano Materials, 2:4, 283-291, DOI: 10.1080/19475411.2011.623728

To link to this article: http://dx.doi.org/10.1080/19475411.2011.623728

International Journal of Smart and Nano Materials
Vol. 2, No. 4, December 2011, 283–291

Taylor & Francis
Taylor & Francis Group

Electrochemical properties of MnO_2/CNT nanocomposite in neutral aqueous electrolyte as cathode material for asymmetric supercapacitors

Hui Xia[a*] and Chao Huo[b]

[a]*School of Materials Science and Engineering, Nanjing University of Science and Technology, Nanjing, Jiangsu 210094, P. R. China;* [b]*National Institute of Metrology China, Bei San Huan Dong Road 18, Beijing 100013, P. R. China*

(*Received 20 June 2011; final version received 12 September 2011*)

A MnO_2/carbon nanotube (CNT) nanocomposite was synthesised using a simple hydrothermal treatment. The nanocomposite exhibits a CNT core/MnO_2 porous sheath hierarchy architecture, which makes it promising as an electrode material for supercapacitors. An asymmetric supercapacitor based on activated carbon (AC) as anode, MnO_2/CNT nanocomposite as cathode and 1M Na_2SO_4 solution as electrolyte was assembled in a Swagelok cell. The full cell exhibits excellent power capability, cycling stability and a high energy density of 23 W h/kg at a power density of 330 W/kg based on the total mass of the active electrode materials. This AC//MnO_2/CNT asymmetric supercapacitor is promising for high-power applications due to its high energy density and power density.

Keywords: supercapacitor; carbon nanotube; nanocomposite

1. Introduction

Energy storage has emerged as one of the major topics alongside the development of alternative energy sources [1,2]. Supercapacitors, also called electrochemical capacitors, with higher energy density compared to traditional electrostatic capacitors and higher power density compared to rechargeable batteries, are promising candidates for next-generation power devices [3]. Currently, most commercial supercapacitors are based on two symmetric activated carbon (AC) electrodes in organic electrolytes [4]. The restriction of aqueous electrolytes is a limited operating voltage of about 1.23 V at which water decomposes. Although organic electrolytes usually can provide a high operating voltage up to 4 V, they have many disadvantages such as low ionic conductivity, high cost, tedious purification processes and flammability. In contrast, aqueous electrolytes have merits in terms of high ionic conductivity, low cost, non-flammability and environmental benignity, which make supercapacitors using aqueous electrolytes more attractive. To further improve the energy density of aqueous electrolyte-based supercapacitor, widening the voltage window is the key. One strategy is to select electrode materials that have high overpotentials for hydrogen and/or oxygen evolutions. Another approach is to combine different positive

*Corresponding author. Email: jasonxiahui@gmail.com

ISSN 1947-5411 print/ISSN 1947-542X online

http://dx.doi.org/10.1080/19475411.2011.623728
http://www.tandfonline.com

and negative electrode materials that have well-separated potential windows to make asymmetric supercapacitors, enabling widening of the cell voltage.

Recently, asymmetric supercapacitors with various anode materials and cathode materials have been extensively investigated to extend the voltage window of aqueous systems [5–8]. For the negative electrode, the material of choice is porous carbon materials due to their low cost, good polarisability and high specific surface area. In the case of positive electrode, Li intercalation compounds, metal oxides and conductive polymers have been investigated as positive electrode materials [5–8]. Among them, MnO_2 with attractive properties such as low cost, high specific capacitance and environment benignity is considered as one of the most promising positive electrode materials [9,10]. Many groups have reported that an asymmetric supercapacitor using MnO_2 and AC as positive and negative electrode, respectively, can operate up to 2 V in aqueous solution [5,6,11,12]. In order to maximise the energy density of the asymmetric supercapacitor, MnO_2 has been synthesised in various nanostructures to increase its specific surface area to obtain a high specific capacitance [13]. However, recent works found that the AC//MnO_2 asymmetric supercapacitors deliver low energy density at high power density indicating poor power capability, which could be attributed to the intrinsically poor electronic conductivity of MnO_2 [14]. To further improve the power capability of the AC//MnO_2 asymmetric supercapacitors, the key is to add conductive additives into nanostructured MnO_2 to improve electron transport of the electrode. Due to their excellent electrical conductivity and high specific surface area, multi-walled carbon nanotubes (CNTs) are now incorporated with MnO_2 to make nanocomposites as electrode materials for supercapacitors [15].

In this work, a facile hydrothermal synthesis has been designed to deposit a uniform and highly porous MnO_2 layer consisting of interconnected nanoflakes onto the surface of the CNTs. An asymmetric supercapacitor was assembled using AC as negative electrode and MnO_2/CNT nanocomposite as positive electrode in a lab-made Swagelok cell. The superior capacitive performance of the AC//MnO_2/CNT asymmetric supercapacitor was investigated and discussed.

2. Experimental

Commercial multi-walled CNTs (20–50 nm in diameter, Shenzhen Nanotech Port Co. Ltd.) were purified by refluxing the as-received sample in 10 wt % nitric acid for 12 h. The acid-treated CNTs were then collected by filtration and dried at 120°C for 12 h in vacuum. A typical synthesis process of the MnO_2/CNT nanocomposite is described as follows. Firstly, 0.1 g CNTs were dispersed in 25 ml deionised (DI) water by ultrasonic vibration for 2 h. 0.3 g $KMnO_4$ was then added into the above suspension and the mixed solution was stirred by magnetic bar for 2 h. After that, the mixed solution was transferred to a 30 ml teflon-lined stainless steel autoclave. The autoclave was sealed and put in an electric oven at 150°C for 6 h and then naturally cooled to room temperature. After the hydrothermal treatment, the resultant samples were collected by filtration and washed with DI water. MnO_2/CNT nanocomposites were finally dried in an oven at 100°C for 12 h for further characterisation.

The crystallographic information of the products was investigated using X-ray diffraction (XRD, Shimadzu X-ray diffractormeter 6000, Cu K_α radiation) with a scan rate of 2°/min and Raman spectra (Jobin-Yvon T6400 micro-Raman system equipped with a charge-coupled device (CCD) detector) using the 514.5 nm line of an Ar^+ laser at a power level of 5 mW. Morphologies of the pristine CNTs and the MnO_2/CNT nanocomposite were characterised by field emission scanning electron microscopy (FESEM, Hitachi

S4300) and transmission electron microscopy (TEM). To prepare the TEM sample, a small amount of MnO_2/CNT nanocomposite was dispersed in ethanol using ultrasonic bath and then was transferred onto the carbon-coated copper grid using a fine pipette.

The electrochemical measurements were carried out on three-electrode cells and two-electrode lab-made Swagelok cells using a Solartron 1287 electrochemical interface. To prepare the positive electrode, 80 wt % of the MnO_2/CNT nanocomposite, 15 wt % carbon black and 5 wt % polyvinylidene difluoride (PVDF) dissolved in *N*-methylpyrrolidone (NMP) were mixed to form a slurry. The slurry was pasted on the Ti foil and dried in a vacuum oven for 12 h. The loading of the working electrode was typically in the range 0.3–0.4 mg ($\sim$ 2 mg cm^{-2}). The AC negative electrode was prepared in the same way as the positive electrode. The weight of the electrode was measured by a microbalance with an accuracy of 0.01 mg. The electrode was composed of carbon black (15 wt %), binder (5 wt %) and MnO_2/CNT nanocomposite (80 wt %). Therefore, the weight of CNT and MnO_2 can be calculated to be 0.24–0.32 mg based on the weight of the electrode. The error could be in the range of $\pm$3–4%. For individual electrode tests in a three-electrode cell, a carbon rod was used as the counter electrode, an Ag/AgCl (saturated KCl) electrode was used as the reference electrode and a 1M Na_2SO_4 solution was used as the electrolyte. For asymmetric full cell tests in a Swagelok cell, a MnO_2/CNT nanocomposite electrode was used as positive electrode, an AC electrode was used as negative electrode and a 1M Na_2SO_4 solution was used as the electrolyte.

3. Results and discussion

The XRD pattern and Raman spectrum of the MnO_2/CNT nanocomposite are shown in Figure 1. As shown in Figure 1a, the XRD pattern can be indexed to the monoclinic potassium birnessite (JCPDS no. 80–1098), which consists of two-dimensional edge-sharing MnO_6 octahedral layers with K^+ cations and water molecules in the interlayer space. The two stronger diffraction peaks correspond to (001) and (002) basal reflections, whereas another two weaker diffraction peaks can be indexed as the (20*l*/11*l*) and (02*l*/31*l*) diffraction bands, respectively. No diffraction peaks from the CNTs can be observed, which is probably due to the coating of the MnO_2 layer. The structural features of the MnO_2/CNT nanocomposite were further investigated using Raman measurements, as shown in Figure 1b. Three Raman bands at 1577 cm^{-1} (G band), 1327 cm^{-1} (D band) and 2652 cm^{-1} (2D band) are observed from Figure 1b for the pristine CNTs, which originate from the Raman-active in-plane atomic displacement E2g mode, disorder-induced features of the CNTs and the overtone of D band [16]. Another three Raman bands located at 501, 575 and 645 cm^{-1} for the MnO_2 are in good agreement with the three major vibrational features of birnessite-type MnO_2 compounds previously reported at 500–510, 575–585 and 625 – 650 cm^{-1} [17]. Therefore, the results of Raman measurements agree well with the XRD results confirming that birnessite-type MnO_2 has been formed during the hydrothermal treatment.

Morphologies of the pristine CNTs and the MnO_2/CNT nanocomposite were characterised by FESEM and TEM, as shown in Figure 2. It can be observed from Figure 2a that the diameter of the CNTs is about 20–50 nm. Figures 2b and 2c show the FESEM images of the MnO_2/CNT nanocomposite at low and high magnifications, respectively. It can be noted that the average diameter of the nanotubes increases for the MnO_2/CNT nanocomposite compared with the pristine CNTs, indicating a thin MnO_2 layer has been coated on the CNT surface. The coated MnO_2 layer is uniform, exhibiting a highly porous structure. Figure 2d shows the TEM image of a single CNT coated with porous

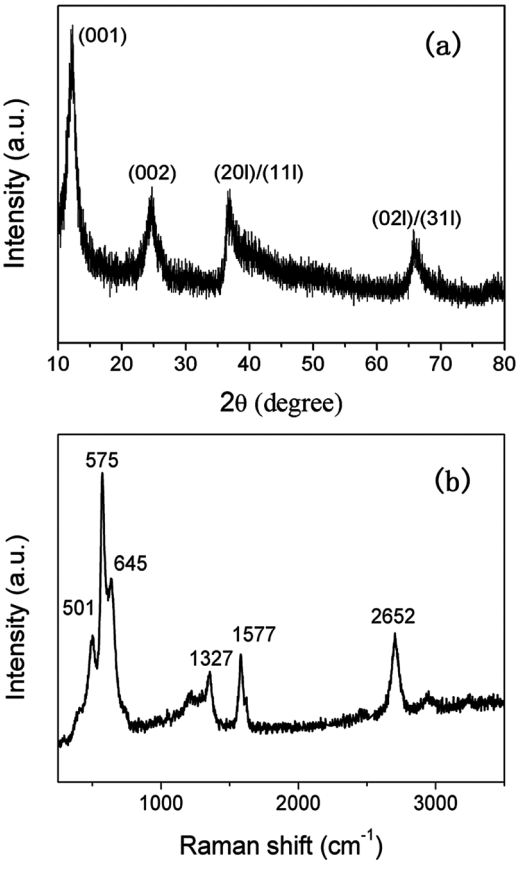

Figure 1. (a) XRD pattern of the MnO_2/CNT nanocomposite. (b) Raman spectrum of the MnO_2/CNT nanocomposite.

MnO_2. The CNT core and the highly porous MnO_2 sheath resemble a caterpillar-like morphology. It can be seen that the porous MnO_2 layer is composed of numerous tiny nanoflakes, which are interconnected and uniformly distributed on the surface of the CNT. The hierarchy architecture and high specific surface area (237 m^2/g by BET analysis) of the MnO_2/CNT nanocomposite make it promising as electrode material for supercapacitors.

Figures 3a and 3b show the cyclic voltammograms (CVs) of the AC and the MnO_2/CNT nanocomposite electrode in 1M Na_2SO_4 aqueous electrolyte at a scan rate of 50 mV/s. The CV of the AC electrode shows an ideal rectangular shape without any noticeable redox peaks from 0 to –1.0 V (vs. Ag/AgCl), which is characteristic of charging/discharging of the electric double layer capacitance. The specific capacitance of the AC electrode is 150 F/g, which agrees well with literature report for commercial AC electrode [18]. The CV of the MnO_2/CNT nanocomposite electrode also exhibits nearly ideal rectangular shape in the voltage range of 0 to 1.0 V (vs. Ag/AgCl) without obvious polarisation. The specific capacitance of the MnO_2/CNT nanocomposite electrode is calculated to be 202 F/g. The specific capacitance of the pristine CNT electrode is only about 20–30 F/g in the same potential range. Therefore, the capacitance of the MnO_2/CNT nanocomposite electrode is mainly contributed by the MnO_2 layer, originating

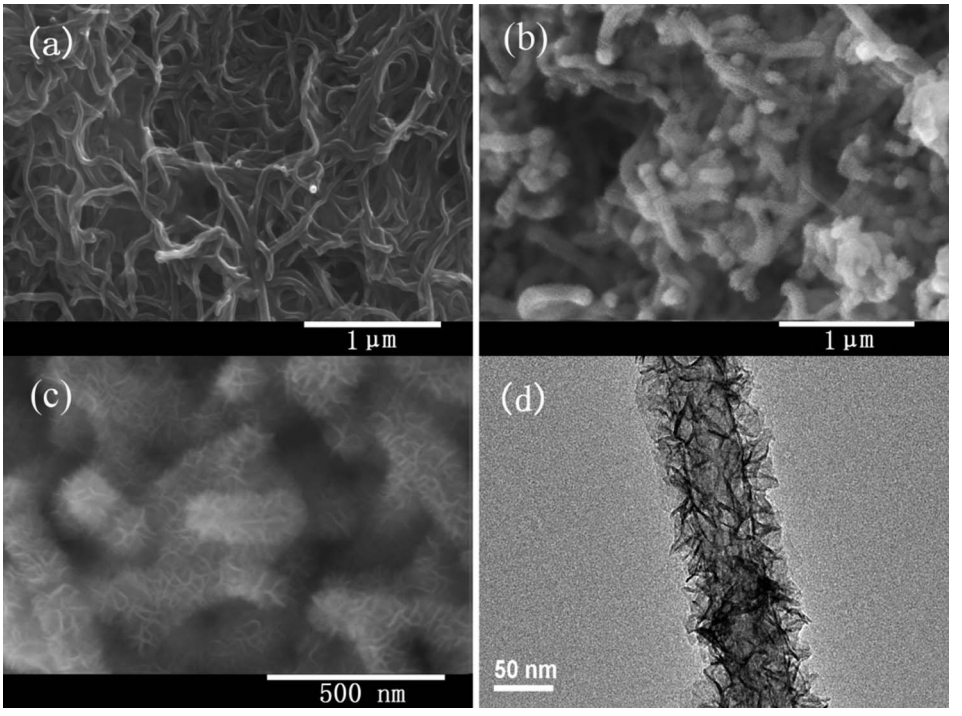

Figure 2. (a) FESEM image of the pristine CNTs. (b, c) FESEM images of the MnO_2/CNT nanocomposite with low and high magnifications. (d) TEM image of a single CNT coated with MnO_2.

from the intercalation–deintercalation of Na^+ into and from the solid lattice. Therefore, an asymmetric supercapacitor, AC//MnO_2/CNT, can be assembled in a two-electrode Swagelok cell using Na_2SO_4 solution as the electrolyte. Figure3c shows the CV of an asymmetric supercapacitor in 1M Na_2SO_4 electrolyte solution at a scan rate of 50 mV/s. The full cell can be stably cycled from 0 to 2.0 V with a nearly ideal rectangular shape, indicating good capacitive feature. It is observed that small slope changes appear at the potential ends in the CV curves in Figure 3. The current leaps become more obvious for active carbon at the negative potential end (Figure 3a) and for MnO_2/CNT nanocomposite at the positive potential end (Figure 3b), which are due to the oxygen evolution at the MnO_2/CNT nanocomposite electrode and hydrogen evolution at the active carbon electrode. As the two electrodes are coupled to build the full cell, a small current leap at the positive potential end (near 2 V, Figure 3c) is due to combination effect of hydrogen and oxygen evolution on both electrodes. The specific capacitance of the AC//MnO_2/CNT asymmetric supercapacitor is calculated to be 40.2 F/g based on the active electrode materials including both cathode and anode, which is higher than the value reported for AC//MnO_2 asymmetric supercapacitors [18]. The high specific capacitance of the AC//MnO_2/CNT asymmetric supercapacitor in the present study could be attributed to the high specific capacitance of the MnO_2/CNT nanocomposite positive electrode, which can match the high specific capacitance of the AC negative electrode. Figure 3d shows the CVs of the AC//MnO_2/CNT asymmetric supercapacitor at different scan rates. It can be seen that the CV curves retain the rectangular shape even at a high scan rate of 200 mV/s, indicating excellent rate capability of the full cell.

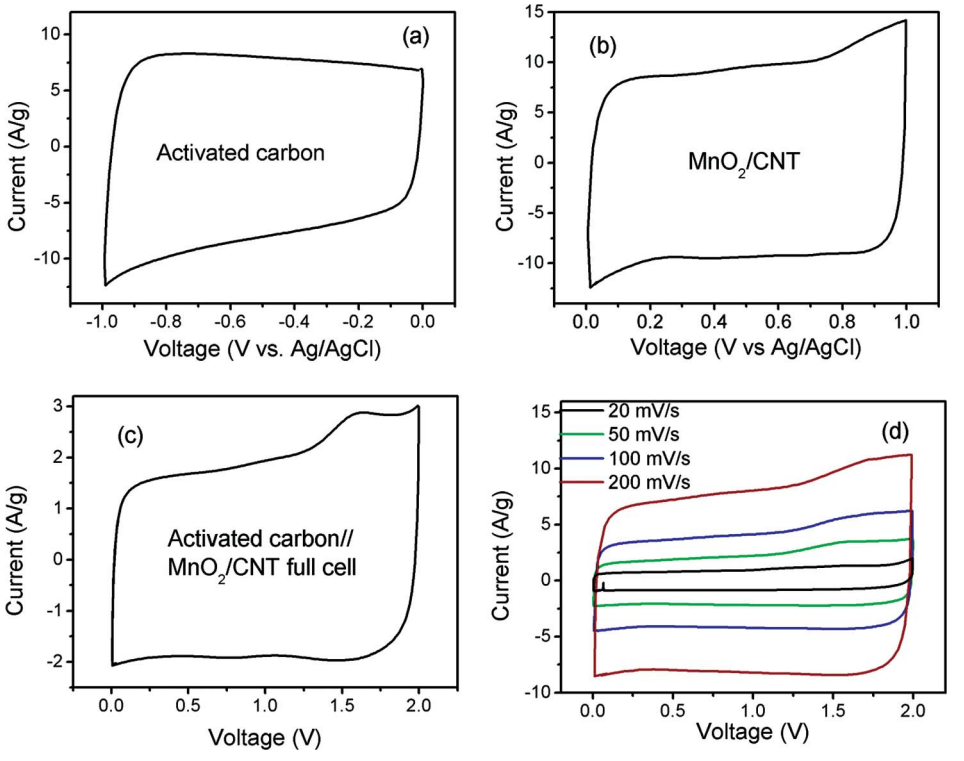

Figure 3. (a) CV curve of the AC electrode in the potential range –1 to 0 V (vs. Ag/AgCl) at a scan rate of 50 mV/s. (b) CV curve of the MnO_2/CNT nanocomposite electrode in the potential range between 0 and 1 V (vs. Ag/AgCl) at a scan rate of 50 mV/s. (c) CV curve of the AC//MnO_2/CNT asymmetric supercapacitor in the potential range between 0 and 2 V at a scan rate of 50 mV/s. (d) CV curves of the AC//MnO_2/CNT asymmetric supercapacitor between 0 and 2 V at various scan rates.

Figure 4a shows the galvanostatic charge/discharge curves of the AC//MnO_2/CNT asymmetric supercapacitor at different current rates ranging from 0.33 to 3.33 A/g. The calculated energy densities and power densities of the full cell at different current rates are given in Figure 4b (Ragone plot). The energy density of the AC//MnO_2/CNT full cell is 23.2 W h/kg at a power density of 330 W/kg, which is higher than that of the AC//AC symmetric supercapacitor and of the AC//MnO_2 asymmetric supercapacitor [11,12]. Theoretically, the cell capacitance, C_{full}, can be calculated based on the following equation:

$$C_{\text{full}} m_{total} V_{\text{full}} = C_{\text{AC}} m_{\text{AC}} V_{\text{half}} + C_{\text{MnO2/CNT}} m_{\text{MnO2/CNT}} V_{\text{half}}, \quad (1)$$

where m_{total} is the sum of m_{AC} and $m_{\text{MnO2/CNT}}$, V_{full} is 2 V, V_{half} is 1 V, C_{AC} is 150 F/g, $C_{\text{MnO2/CNT}}$ is 202 F/g. C_{full} can be calculated to be about 50 F/g. The energy density, $E_{\text{full}} = 1/2 C_{\text{full}} V_{\text{full}}^2$, can be calculated to be 27.7 W h/kg, which is a little larger than the experimental value of 23.3 W h/kg. Most importantly, the AC//MnO_2/CNT asymmetric supercapacitor exhibits superior power capability compared to the AC//MnO_2 asymmetric supercapacitor, as shown in Figure 4b. The AC//MnO_2 asymmetric supercapacitor can also deliver a high energy density of nearly 20 W h/kg at a low power density of about

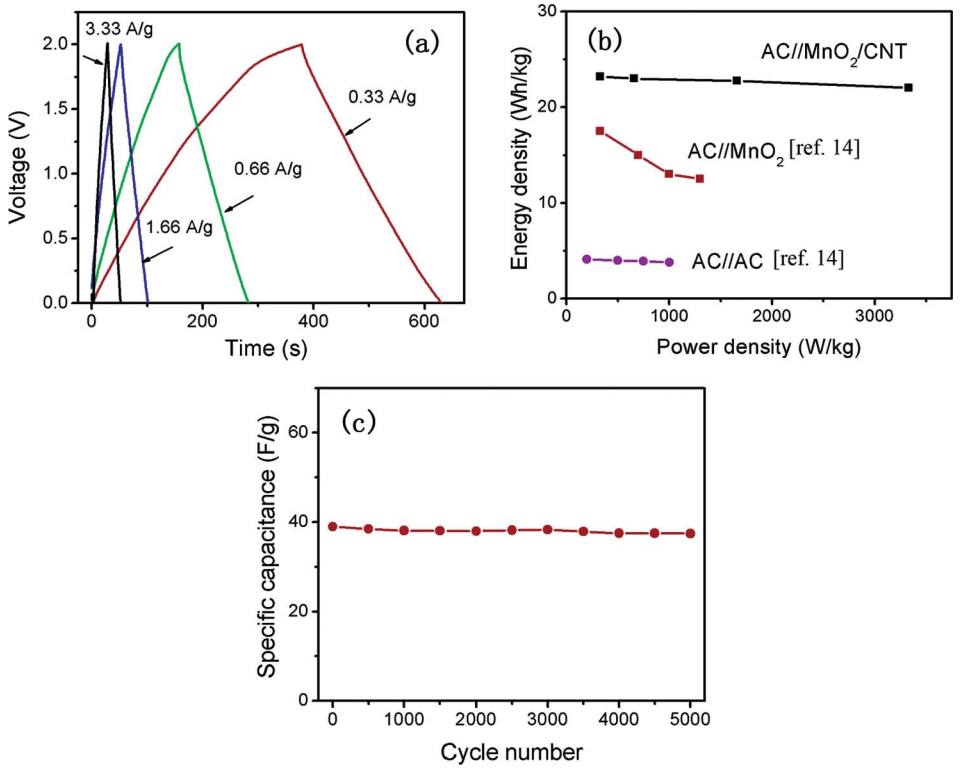

Figure 4. (a) Charge/discharge curves of the AC//MnO_2/CNT asymmetric supercapacitor between 0 and 2 V at various current rates. (b) Ragone plots of the AC//MnO_2/CNT asymmetric supercapacitor, the AC//MnO_2 asymmetric supercapacitor [14], and the AC//AC symmetric supercapacitor [14]. (c) Cycle performance of the AC//MnO_2/CNT asymmetric supercapacitor.

100 W/kg [14]. However, the energy density of the full cell decreases quickly as the power density increases. At a high power density of 1 kW/kg, the AC//MnO_2 full cell can only retain an energy density of 13.2 W h/kg [14]. In contrast, the AC//MnO_2/CNT full cell can retain an energy density of 22 W h/kg at a power density of 3 kW/kg, indicating significantly improved power capability compared to the AC//MnO_2 full cell.

The rate limiting steps for the MnO_2-based electrode could be the Na^+ ion diffusion and electron diffusion in MnO_2. As MnO_2 is intrinsically a poor electron conductor and the Na^+ diffusion only occurs at the surface of the MnO_2, if the particle size of MnO_2 is big, the electrode will exhibit poor rate capability due to the sluggish transport of electron and Na^+ ion in MnO_2. As Na^+ ion has much higher ion conductivity in solution than in solid, the Na^+ ion transport in the electrolyte could not be the rate limiting step. The superior power capability of the AC//MnO_2/CNT asymmetric supercapacitor can be explained by the unique nanoarchitecture of the MnO_2/CNT nanocomposite. First, each MnO_2 nanoflake grows directly on the CNT surface. The CNTs construct a three-dimensional (3D) highly conductive current collector, which significantly increases the electronic conductivity of the nanocomposite. Second, the large specific surface area and the nanoscopoic MnO_2 phase of the MnO_2/CNT nanocomposite minimise the solid state transport distances for both ions and electrons. This ensures a high utilisation of the electrode material, a high specific capacitance and a good rate capability. Third, the highly porous structure of the

MnO_2 layer is able to minimise the diffusion distance of the electrolyte to the interior surfaces of MnO_2, which facilitates better penetration of electrolyte into the electrode material and enhances the ionic conductivity of the electrode material. The birnessite-type MnO_2 has a layered structure, which is stable during long-term intercalation/deintercalation of Na^+ [14]. The cycle performance of the AC//MnO_2/CNT asymmetric supercapacitor is shown in Figure 4c. After 5000 cycles at a current rate of 1.6 A/g between 0 and 2.0 V, only a slight capacitance loss (< 5%) is observed for the full cell, indicating good cycling stability of the AC//MnO_2/CNT asymmetric supercapacitor.

4. Conclusions

A MnO_2/CNT nanocomposite with a CNT core/MnO_2 porous sheath hierarchy architecture has been successfully designed as positive electrode for AC//MnO_2/CNT asymmetric supercapacitor using neutral aqueous electrolyte. The asymmetric supercapacitor using MnO_2/CNT nanocomposite as positive electrode exhibits high specific capacitance, high energy density, excellent power capability and good cycling stability. The superior capacitive performance of the AC//MnO_2/CNT asymmetric supercapacitor is due to the unique nanoarchitecture of MnO_2/CNT nanocomposite, which facilitates fast electron and ion transport. The AC//MnO_2/CNT asymmetric supercapacitor has high application potential in large power devices due to its high energy density and power density.

Acknowledgement

This research is supported by Nanjing University of Science and Technology through the research grant NUST Research Funding (AB41385 and 2011ZDJH21).

References

[1] J. Liu, H. Xia, D.F. Xue, and L. Lu, *Double-shelled nanocapsules of V_2O_5-based composites as high-performance anode and cathode materials for Li ion batteries*, J. Am. Chem. Soc. 131 (2009), pp. 12086–12087.

[2] J. Liu and D.F. Xue, *Sn-based nanomaterials converted from SnS nanobelts: facile synthesis, characterizations, optical properties and energy storage performances*, Electrochim. Acta 56 (2010), pp. 243–250.

[3] P. Simon and Y. Gogotsi, *Materials for electrochemical capacitors*, Nat. Mater. 7 (2008), pp. 845–864.

[4] A. Burke, *R&D considerations for the performance and application of electrochemical capacitors*, Electrochim. Acta 53 (2007), pp. 1083–1091.

[5] Z.S. Wu, W.C. Ren, D.W. Wang, F. Li, B.L. Liu, and H.M. Cheng, *High-energy MnO_2 nanowire/graphene and graphene asymmetric electrochemical capacitors*, ACS Nano 4 (2010), pp. 5835–5842.

[6] Q.T. Qu, Y. Shi, L.L. Li, W.L. Guo, Y.P. Wu, H.P. Zhang, S.Y. Guan, and R. Holze, *$V_2O_5.0.6H_2O$ nanoribbons as cathode material for asymmetric supercapacitor in K_2SO_4 solution*, Electrochem. Comm. 11 (2009), pp. 1325–1328.

[7] J.W. Lang, L.B. Kong, M. Liu, Y.C. Luo, and L. Kang, *Asymmetric supercapacitors based on stabilized alpha-$Ni(OH)_2$ and activated carbon*, J. Solid State Electrochem. 14 (2010), pp. 1533–1539.

[8] Y. Zhao, Q.Y. Lai, Y.J. Hao, and X.Y. Ji, *Study of electrochemical performance for AC/$(Ni_{1/3}Co_{1/3}Mn_{1/3})(OH)_2$*, J. Alloy Comp. 471 (2009), pp. 466–469.

[9] D.Y. Cui, K. Gao, P. Lu, H. Yang, Y.N. Liu, and D.F. Xue, *Mild solution route to mixed-phase MnO_2 with enhanced electrochemical capacitance*, Funct. Mater. Lett. 4 (2011), pp. 57–60.

[10] W.F. Wei, X.W. Cui, W.X. Chen, and D.G. Ivey, *Manganese oxide-based materials as electrochemical supercapacitor electrodes*, Chem. Soc. Rev. 40 (2011), pp. 1697–1721.

[11] Q.T. Qu, L. Li, S. Tian, W.L. Guo, Y.P. Wu, and R. Holze, *A cheap asymmetric supercapacitor with high energy at high power: activated carbon//$K_{0.27}MnO_2.0.6H_2O$*, J. Power Sourc. 195 (2010), pp. 2789–2794.

[12] Q.T. Qu, P. Zhang, B. Wang, Y.H. Chen, S. Tian, Y.P. Wu, and R. Holze, *Electrochemical performance of MnO_2 nanorods in neutral aqueous electrolytes as a cathode for asymmetric supercapacitors*, J. Phys. Chem. C 113 (2009), pp. 14020–14027.

[13] H. Xia, M.O. Lai, and L. Lu, *Nanostructured manganese oxide thin films as electrode material for supercapacitors*, J. Miner. Met. Mater. Soc. 63 (2011), pp. 54–59.

[14] Q.T. Qu, Y. Shi, S. Tian, Y.H. Chen, Y.P. Wu, and R. Holze, *A new cheap asymmetric aqueous supercapacitor: activated carbon//$NaMnO_2$*, J. Power Sourc. 194 (2009), pp. 1222–1225.

[15] F. Feng, S. Santhanagopalan, Y. Wang, and D.D. Meng, *In-situ hydrothermal synthesis of three-dimensional MnO_2–CNT nanocomposites and their electrochemical properties*, J. Alloy Comp. 499 (2010), pp. 259–264.

[16] X.F. Xie and L. Gao, *Characterization of a manganese dioxide/carbon nanotube composite fabricated using an in situ coating method*, Carbon 45 (2007), pp. 2365–2373.

[17] A. Ogata, S. Komaba, R. Baddour-Hadjean, J.P. Pereira-Ramos, and N. Kumagai, *Doping effects on structure and electrode performance of K-birnessite-type manganese dioxides for rechargeable lithium battery*, Electrochim. Acta 53 (2008), pp. 3084–3093.

[18] P.C. Gao, A.H. Lu, and W.C. Li, *Dual functions of activated carbon in a positive electrode for MnO_2-based hybrid supercapacitor*, J. Power Sourc. 196 (2011), pp. 4095–4101.